IEEE Access
Multidisciplinary | Rapid Review | Open Access Journal

Received May 10, 2019, accepted June 8, 2019, date of publication June 19, 2019, date of current version July 10, 2019.

Digital Object Identifier 10.1109/ACCESS.2019.2923836

A High-Precision Hybrid Analog and Digital Beamforming Transceiver System for 5G Millimeter-Wave Communication

RUOQIAO ZHANG, (Student Member, IEEE), JIANYI ZHOU, (Member, IEEE), JI LAN, BINQI YANG, (Student Member, IEEE), AND ZHIQIANG YU, (Member, IEEE)
State Key Laboratory of Millimeter-Wave, Southeast University, Nanjing 210096, China
Corresponding author: Jianyi Zhou (jyzhou@seu.edu.cn)

ABSTRACT In this paper, the development of a millimeter-wave hybrid beamforming (HBF) transceiver system for 5G millimeter-wave multiple-input–multiple-output (MIMO) communication is presented. The developed transceiver system is operated at 28-GHz band in the time division duplex (TDD) mode, with 500-MHz signal bandwidth. To implement high beamforming accuracy, a phased-array-based HBF transceiver with high-precision phase shifting network (PSN) at intermediate-frequency (IF)-paths is proposed. The designed PSN has 8-bit phase resolution within 360° range and 0.13-dB amplitude variation. With the use of such low-cost 8-bit PSN, this HBF transceiver system achieves 0.6° beam resolution and a good RF transceiver performance. In addition, under the over-the-air MIMO communication test with two data streams, the error vector magnitude (EVM) of the received signals at two user equipment (UE) is 2.58% and 2.34%. The high-data rate millimeter-wave communication and MIMO performance of this HBF are verified.

INDEX TERMS Hybrid beamforming, MIMO, millimeter-wave, transceiver, phased array.

I. INTRODUCTION

With the development of communication system technology, providing wider radio frequency (RF) bandwidth by utilizing millimeter-wave (mmWave) bands is a promising solution for 5G massive multiple-input multiple-output (MIMO) communication [1]–[3]. Different from conventional communication systems in sub-6GHz frequency bands, mmWave bands promise great features like increased data transmission rate and improved spectrum efficiency.

In order to overcome the increased path loss at higher frequency bands and realize multi-users communication, the beamforming technology with steerable radiation pattern and high gain characteristics is required. Recently, many potential beamforming architectures have been proposed and analyzed, including analog beamforming architecture, fully digital beamforming architecture [4] and hybrid beamforming architecture [5]–[8]. Although the fully-digital beamforming (DBF) architecture can offer the greatest flexibility and performance, the DBF has some unavoidable problems, such as high cost level and huge power consumption. Therefore, hybrid analog-digital beamforming (HBF) with a reduced number of digitized chains and digital process units are gradually applied on the base station (BS) system [9]. In this HBF architecture, as shown in Fig. 1(b), the digital beamforming is performed in digital process unit, such as field-programmable gate array (FPGA), whereas the analog beamforming is implemented by analog phased array [10], [11]. Unlike DBF requiring one digitized chain for each antenna element, the HBF architecture replaces most of digitized chains with the phased array sub-array. So the number of FPGA, DAC, ADC and IF transceiver can be greatly reduced [12].

Recently, several advanced techniques have been developed to improve the performance of HBF system to approach the DBF performance as close as possible. Among them, the analog precoding matrix optimization algorithm or employing a limited number of simple phase over-sampler can be achieved in low-resolution phase shifting network to maintain satisfactory spectral efficiency [13]–[16]. The other method is to develop the phased array with high precision and low cost phase shifting network (PSN) for HBF system [17]. There exist many advanced phased array architectures proposed for HBF [18]–[22], such as the passive

The associate editor coordinating the review of this manuscript and approving it for publication was Debashis De.

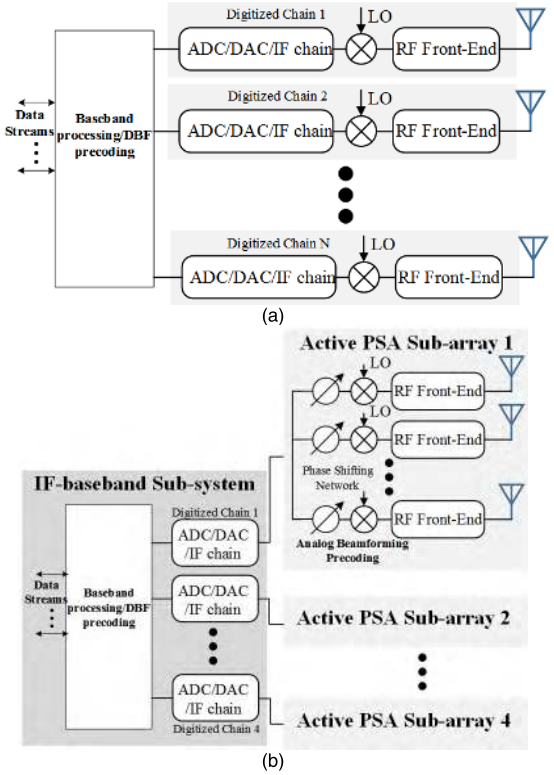

FIGURE 1. Simplified block diagram of the (a) fully DBF transceiver array and (b) hybrid beamforming transceiver array with IF-path PSN.

multi-beam array in [18], [19], the lens-based Butler matrix multi-beam array [20] and the active phased array [21], [22]. Among them, when putting passive beam switching circuits between the RF front-end and antenna, the passive multi-beam array or Butler matrix based array introduce extra noise and insertion loss, which will reduce the dynamic range and decrease the coverage distance of the transceiver. Thus, the active phased array can offer higher transmission power and better receive sensitivity to satisfy the coverage of cell edge area. In the aspect of PSN, several works based on integrated phase shifters have been reported in [23], [24]. However, the phase shifting resolution of the phase shifter chips used in mmWave bands is only 5 bits or 6 bits. Besides, these phase shifters have significant amplitude fluctuation which affects the performance of transceiver system. Another serious problem caused by low-resolution phase shifter is the blind area of coverage. Low phase resolution will cause large beam steering step. As a result, the blind area of coverage occurs when using a large-scale phased array to form high direction gain but narrow beam. Therefore, the high precision active phased array can provide a complete coverage for massive MIMO HBF communication.

In this paper, a mmWave band HBF communication transceiver system with IF-path high precision PSN is presented. This mmWave MIMO HBF transceiver system is operated at 28GHz band in time division duplex mode, with 500MHz signal bandwidth. In this phased array, the IF-path PSN approach is employed to obtain high precision and low cost. The proposed novel vector-sum phase-shifting unit used in PSN has 8-bit phase resolution within 360° phase shifting range and 0.13dB amplitude variation. The final test results show good beam resolution and RF transceiver performance of this transceiver system. In addition, the high data rate transmission capability of the HBF system is verified by the indoor over-the-air MIMO communication test. This paper is organized as follows. Section II describes the influence of the RF chain vector error and phase resolution on the radiation beam pattern, and presents the architecture of this HBF transceiver system. Section III presents detailed design of the elemental component parts in transceiver system, such as IF-baseband subsystems and the phased array which contains four vertically-placed phase shifting sub-arrays and one local oscillator (LO) subsystem. Section IV gives the achieved test results of hardware performance and experimental results of whole mmWave HBF MIMO communication system. The conclusion would be covered in Section V finally.

II. THE ANALYSIS AND ARCHITECTURE OF MMWAVE HBF TRANSCEIVER SYSTEM

In multi-user HBF communication system, the data streams are first digitally modified in IF-baseband subsystem by digital precoding matrix $\mathbf{W}_D$. Moreover, the processed signals are up-converted and achieved analog beamforming using analog precoding matrix $\mathbf{W}_R$. Therefore, after transmitted through air channels, the received signal at k-th user can be written as [10]

$$\mathbf{y} = \mathbf{H}(\sum_{i=1}^{K} \mathbf{W}_R \mathbf{W}_{D_i} \mathbf{s}_i + \mathbf{n}), \tag{1}$$

$$\mathbf{y} = \mathbf{H}\mathbf{W}_R \mathbf{W}_{D_k} \mathbf{s}_k + \mathbf{H} \sum_{i \neq k} \mathbf{W}_R \mathbf{W}_{D_i} \mathbf{s}_i + \mathbf{n}, \tag{2}$$

where $\mathbf{H} = [\mathbf{h}_1, \ldots, \mathbf{h}_K]$ is the normalized air interface response matrix of channel information from the BS to the k-th user, $\mathbf{s} \in \mathbb{C}^{K \times 1}$ is the transmission symbol of all data streams, $\mathbf{n} \in \mathbb{C}^{K \times 1}$ is the vector of i.i.d $CN(0, N_0)$ noise and N_0 is the noise power. According to (2), the real-time air channel information $\mathbf{H}$ can be estimated through pilot training. With the perfect knowledge of channel information $\mathbf{H}$, previous studies discussed lots of methods used for calculating the optimal hybrid precoding matrix in HBF system [8], [25]. However, the effects of actual transceiver hardware system, especially of active phased array, are not taken into account in these design models. In this section, the influence of RF chain vector error to the final beam pattern in the analog PSN is analyzed firstly. In addition, the architecture of this high precision HBF transceiver system is presented.

A. THE ANALYSIS OF RF CHAIN VECTOR ERROR IN HBF SYSTEM

The simplified block diagram of the HBF system is demonstrated in Fig. 1(b). In multi-user communication, other data streams in the space becomes the interference of the target

user, and the received signal to interference plus noise (SINR) of k-th user can be written as

$$\gamma_k = \frac{\left\|\mathbf{h}_k^H \mathbf{W}_k\right\|^2}{\sum_{\zeta \neq k}\left(\left\|\mathbf{h}_k^H \mathbf{W}_\zeta\right\|^2\right) + N_0^2} \xrightarrow{\mathbf{h}_k^H \mathbf{W}_\zeta = \theta} \frac{\left\|\mathbf{h}_k^H \mathbf{W}_k\right\|^2}{N_0^2}. \quad (3)$$

where the ζ represents the any other user except k-th user, the $\mathbf{W}_\zeta$ means the precoding matrix of user ζ. When the optimal precoding matrix is applied to HBF system, the signal received in user equipment (UE) has the highest signal to interference plus noise (SINR). That means the whole system generates N orthogonal beams in the space, and the main lobe of each beam is pointing to the target user while the zero points of the beam point to other users. Therefore, in communication scenario, the beam zero-points suppression and distribution need to be carefully considered and valued. In HBF, however, the analog beamforming is achieved by the PSN, which introduces the amplitude fluctuation and phase shifter precision error in each RF chains to greatly affect the zero-points distribution. In order to clearly see the influence from hardware error to the beam pattern, this PSN is assumed to have a vector error including phase error Φ_n and amplitude error σ_n at nth RF chain in normal distribution. As indicated above, N elements uniform linear array at one dimensional far-field radiation pattern can be written as

$$F(\phi) = p(\phi) \sum_{n=0}^{N-1} a_n \left(1 + \delta_n\right) e^{-j2\pi n \frac{d}{\lambda_0} \sin\phi + \Phi_n}, \quad (4)$$

where ϕ is the azimuth angle of the beam directivity, d is the antenna adjacent distance, λ_0 is the wavelength of signal, $p(\phi)$ is the single antenna radiation pattern and a_n is complex excitation at the n-th radiation element. Let ξ donates the $\sin\phi$, that $\phi \in [-90°, 90°]$. The array factor can be viewed as the district Fourier transform (DFT) from one spatial discrete excitation sequence $\{a_n\}$ with the complex vector error $\{b_n\}$ to spectrum domain [4]:

$$F(\xi) = \sum_{n=0}^{N-1} \left(a_n + b_n\right) e^{-j2\pi n \frac{d}{\lambda_0} \xi}, \quad (5)$$

where

$$b_n = \delta_n e^{-j\Phi_n}. \quad (6)$$

With the DFT, the complex vector error sequence $\{b_n\}$ transforms to the error spectrum, which is illustrated in Fig. 2(a). As is shown in Fig. 2(a), error spectrum has less effect on the main beam gain and directivity, but it greatly influents the distribution of the side-lobes and zero-points of the beam. Because of the randomness of the error sequence, 100 times simulations are performed on the phase error, and the envelope of the results is drawn in the Fig. 2(b) to demonstrate the error spectrum influence on the beam. Therefore, when the 13.2° root mean square (RMS) phase error is added in each RF chains, the suppression at the zero-points is deteriorated to 15dB, which means the SINR is

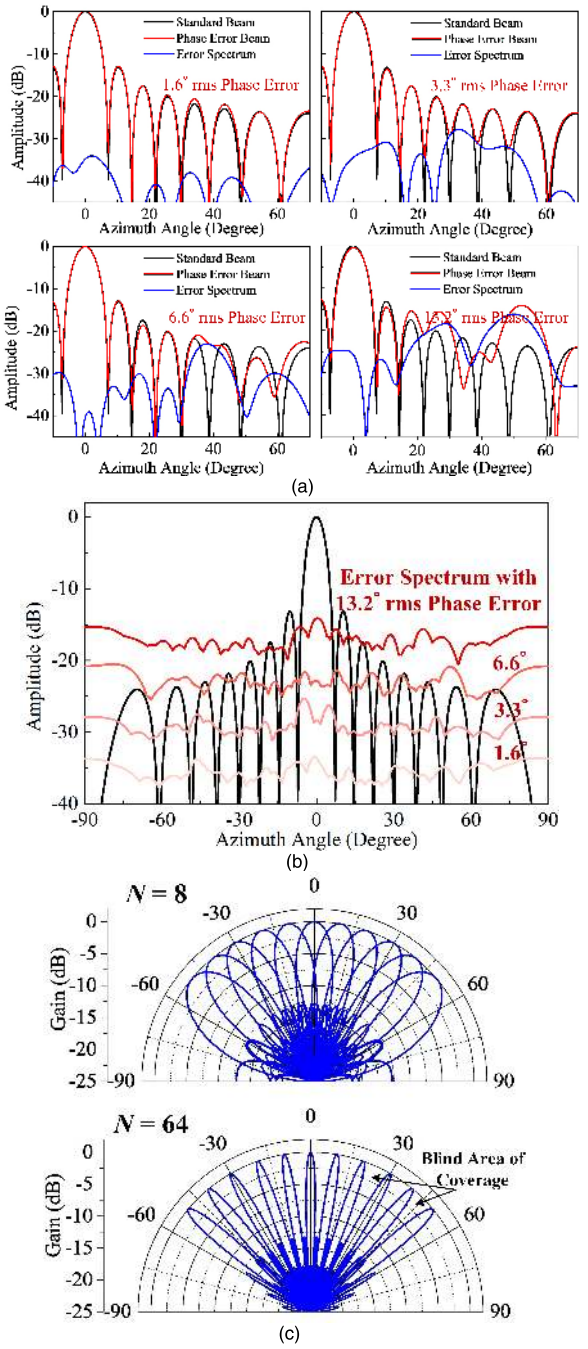

FIGURE 2. (a) The beam pattern comparison before and after adding different phase error perturbation, (b)the error spectrum with different phase error, and (c) the comparison of beam patterns at different array scale.

greatly deteriorated. As demonstrated in Fig. 2(b), holding that zero-points suppression to a degree of 30dB requires RMS phase error of only 1.6°.

In addition, the beam steering resolution $\Delta\theta$ in space depends on the phase resolution $\Delta\phi$ of the PSN, that can be indicated in [7]

$$\Delta\theta = \arcsin\left(\frac{\lambda_0}{2\pi d}\Delta\phi\right). \quad (7)$$

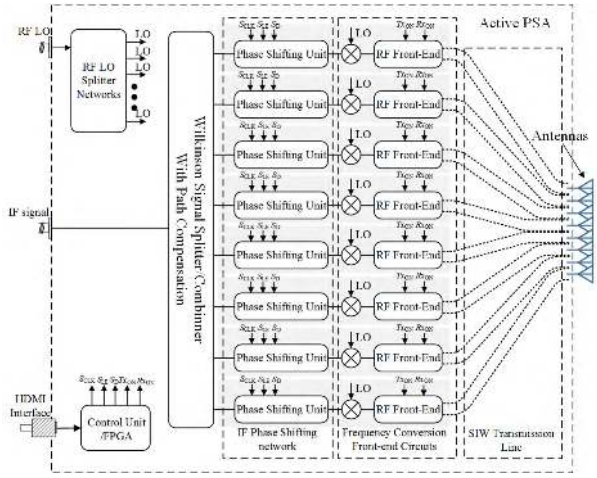

FIGURE 3. The block diagram of one sub-array in phased array.

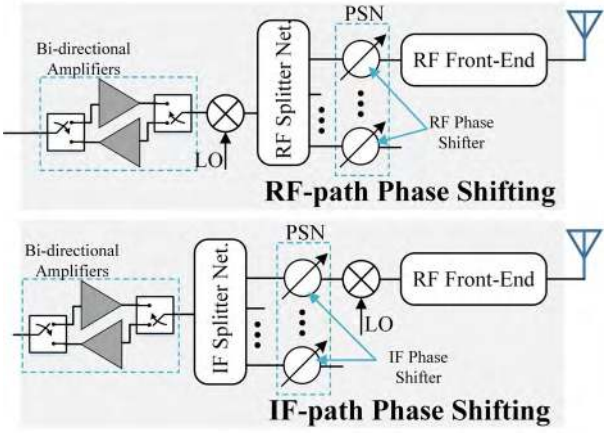

FIGURE 4. The block diagram of RF-path phase shifting and IF-path phase shifting architectures.

In antenna array, the beam-width of main beam F_0 is defined as the angle between the zero-points on the both sides of the main beam:

$$F_0 = 2\arcsin(\frac{2\lambda_0}{Nd}), \tag{8}$$

where N is the number of the antennas in this dimension, d is the distance between adjacent antennas. As the scale of the antenna array is getting larger, the beam-width of main beam will be narrower. As illustrated in Fig. 2(c), large scale array with low phase resolution generates the beam pattern blind area of coverage. So that the increasing channel loss impacts on the transmission rate of mobile communication in the blind area of coverage. It is necessary to apply high precision PSN in HBF to reduce the unrelated data stream interference and eliminate the blind area of coverage.

B. PROPOSED MILLIMETER-WAVE HBF TRANSCEIVER SYSTEM ARCHITECTURE

According to the above analysis, the proposed transceiver system hardware architecture for mmWave large scale MIMO is designed. The mmWave HBF MIMO transceiver system has two main parts, the mmWave active phased array and IF-baseband subsystem, which are shown in Fig. 1(b).

This 32 RF-chains active phased array is grouped into four uniform linear sub-arrays which are placed vertically and one LO subsystem. Each digitized chain in IF-baseband subsystem connects with one phased sub-array containing eight RF chains and eight antennas. Fig. 3 illustrates the simplified block diagram of the proposed phased sub-array architecture. This mmWave active phased sub-array consists of IF PSN, IF signal power splitter/combiner network with path compensation and frequency conversion front-end circuits with radiation elements. In order to obtain high phase resolution and low amplitude fluctuation, the IF-path PSN architecture with novel vector-sum phase shifting unit is adopted. One FPGA chip is integrated for the control of the PSN and the transceiver switching, which is communicated with the baseband unit through high speed serial peripheral interface (SPI) lines.

The IF-baseband subsystem in this HBF system not only provides digital beamforming for baseband signal, but also up-converts the baseband signal to IF band and implements IF signal gain controlling. The IF signal has a carrier frequency of 2.75GHz with 500MHz signal bandwidth. The IF transmitter directly up-converts to 2.75GHz by wideband quadrature modulator. It also supports the fine tuning of IF oscillator leakage through the bias voltage adjustment. By utilizing under-sampling technology, the IF receiver directly samples and digitally down-converts the IF signal, to eliminate the error caused by demodulator and simplify the receiver circuits. To satisfy the sufficient linear output power of different distance between base station and UE, both IF transmitter and receiver have gain control components for adjusting the output signal amplitude and power.

The LO subsystem is placed at the side of the phased array. This LO subsystem provides 100MHz, 2.754GHz (IF LO frequency) and 12.6GHz (RF LO frequency). In order to decrease the phase noise of LO, dual-loop phase locked loop (PLL) structure is proposed in this design. In addition, one oven controlled crystal oscillator (OCXO) is used for high phase noise performance LO design.

C. ADVANTAGES AND CONSTRAINS OF THE PROPOSED IF-PATH PSN ARCHITECTURE

Fig. 4 illustrates the RF-path phase shifting architecture and IF-path phase shifting architecture, respectively. In the traditional RF-path architecture, by using phase shifter in mmWave, the output signal can be expressed as

$$D_{\mathrm{RF}}(t) = D_{\mathrm{BB}}(t)e^{j(\omega_{\mathrm{RF}}t+\phi_{\mathrm{RF}})}, \tag{9}$$

where $D_{\mathrm{BB}}(t)$ is the complex baseband signal, ω_{RF} is the RF carrier frequency and ϕ_{RF} is the shifted phase by the RF-path phase shifter. When IF-path PSN is taken into consideration,

TABLE 1. Comparison of cost and power consumption in different architectures.

Module	Cost (USD $)	Power consumption	Number in DBF	Number in HBF_1[b]	Number in HBF_2[c]
Front-end[a]	High /161	High	32	32	32
Mixer	Low /16	Low	32	4	32
RF Phase Shifter	High /170	Low	0	32	0
IF-path PSU	Low /14	Low	0	0	32
DAC /ADC	Mid. /55	High	32	4	4
FPGA	High /714	High	32	4	4

[a] RF front-end means a standard mmWave front-end circuits which contain PA, LNA, driver amplifier, LO amplifier and two RF switches.
[b] RF phase shifter is used as the analog beamforming in HBF_1 system architecture.
[c] The IF-path phase shifting unit is used as the analog beamforming in HBF_2 system that is designed in this work.

the output RF signal can be given as follows,

$$D_{RF}(t) = D_{BB}(t)e^{j(\omega_{IF}t+\phi_{IF})} \cdot e^{j(\omega_{LO}t+\phi_{LO})} = D_{BB}(t)e^{j(\omega_{RF})t} \cdot e^{j(\phi_{IF}+\phi_{LO})}, \quad (10)$$

where ϕ_{IF} is the phase of the IF-path, ϕ_{LO} is the phase of the LO-path, ω_{IF} is the IF carrier frequency and ω_{LO} is the LO signal frequency. Therefore, by providing in-phase LO signals to different chains, there is no difference in phase shifting performance between RF-path and IF-path phase shifting structures.

However, the proposed IF-path phased array architecture has several advantages. Firstly, IF-path phase shifting has fine phase shifting resolution with low amplitude fluctuation across the whole phase shifting state. The vector-sum phase shifting unit is used in this IF-path PSN architecture, which is to weight the amplitude of two orthogonal-phased input signals (I-path and Q-path) for synthesizing the required phase. Due to the lower frequency band, the quadrature coupler has more accurate phase difference between I-path and Q-path. Moreover, the amplitude weighting device can approach 31.75dB amplitude weighting range with 7-bit control step of result in fine phase shifting value.

Secondly, a significant advantage of the IF-path phase shifting is the low cost. In microwave circuits, the price of chips is proportional to the operation frequency band. The RF carrier frequency of designed system is 28GHz, while the IF carrier frequency is 2.75GHz. As illustrated in Table 1, compared with fully DBF and other HBF architectures with mmWave bands phase shifters, the cost and power consumption of this IF-path PSN transceiver system are greatly decreased.

In addition, IF-path phase shifting structure has higher linear output power in each RF chain. As shown in Fig. 4,

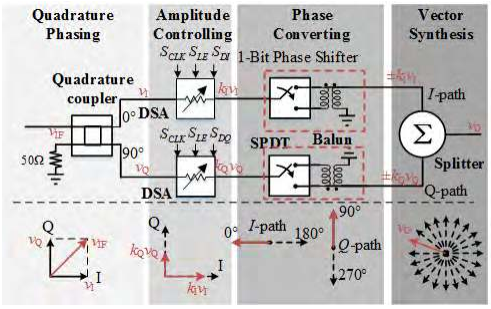

FIGURE 5. The schematic and principle of proposed phase shifting unit in phased array.

the maximum linear output power of the RF front-end is limited by the passive mixer nonlinearity (usually mixer linear output power is −10dBm at 10dB back-off). In the RF-path phase shifting, the RF splitter network and RF phase shifter have total 19.5dB insertion loss, which decrease the linear transmitted power of front-end. In contrast, in IF-path phase shifting architecture, the insertion loss between the mixer and RF front-end input port is moved to the IF-path, which has no effect on the output power linearity.

One of the major constraints of this passive IF-path phase shifting architecture is the large insertion loss. Therefore, as shown in Fig. 4, the bidirectional amplifiers are utilized in IF-path for compensating the insertion loss, which does not result in a significant increase in cost. Another limitation is the relationships between the control signals (amplitude weighting control) and output phase of this vector-sum phase shifting unit are not linear, which makes the design of the control circuits quite complex. Thus, in each phased sub-array, the PSN is controlled by one FPGA storing with calibrated linear phase table to simplify the control circuits.

III. DESIGN OF TRANSCEIVER ELEMENTAL COMPONANT

A. DESIGN OF THE PHASED ARRAY

1) PHASE SHIFTING NETWORK DESIGN

The most important part in this phased array is the IF-path PSN that contains eight 8-bit phase resolution phase shifting units. This phase shifting unit is designed based on the novel vector-sum architecture. The schematic and layout of this phase shifting unit are shown in Fig. 5. The proposed 8-bit phase shifting unit consists of digital step attenuator, quadrature coupler, 1-bit phase shifter and power splitter. Compared with other vector-sum phase shifters [26], [27], this is one passive phase shifting unit that can achieve good signal linearity without consuming any DC power. Besides, this phase shifting unit is bi-directional, thus can be shared in between transmitter and receiver to save half number of phase shifting units.

The digital step attenuator (DSA) is used as the amplitude control component in the unit instead of the gain control amplifier, which makes the vector-sum phase shifter bidirectional. This DSA (PE43711) has up to 31.75dB controllable amplitude range that minimizes the range of unreachable

phase angle. And the attenuation step of this DSA is 0.25dB, which makes this phase shifter having high phase shifting resolution and low amplitude fluctuation. Moreover, the 1-bit phase shifter is used to achieve the fast switching between different quadrants, so that the phase range of this phase shifting unit can cover 360°. This 1-bit phase shifter consist of single-pole double-throw (SPDT) switch and wideband 1:1 balun (transmission line transformer). By switching the dotted terminal and the invert terminal of the balun, the phase of the IF path can be inverted. Because of the less phase unbalance introduced by 1-bit phase shifter, the amplitude fluctuation at whole phase range has been improved. As shown in Fig.5, the phasor diagrams at the bottom of schematic illustrate how a representative input signal is modified as it propagates through the phase shifter. The input IF signal v_{IF} can be constructed by combing two orthogonal signals, v_{I} and v_{Q}, for the I-path and Q-path, respectively. A pair of DSAs are used to modify the magnitude of these two orthogonal signals with the coefficients k_{I} and k_{Q}. Two 1-bit phase shifters provide phase converting in I-path (0° or 180°) and in Q-path (90° or 270°). After that, with the power splitter, v_{I} and v_{Q} are combined together to generate the signal with desired output phase and amplitude.

With the IF-path bi-directional amplifier, this IF-path phase shifting unit obtain the gain to increase the signal to noise ratio. Finally, the voltage of output signal v_{O} can be written as

$$v_{\mathrm{O}}(t) = \pm G_{\mathrm{A}} L_{\mathrm{O}} \left(k_{\mathrm{I}} v_{\mathrm{I}} \pm j k_{\mathrm{Q}} v_{\mathrm{Q}}\right) e^{j(wt+\varphi)}, \tag{11}$$

where the constant coefficient L_{O} is the induced insertion loss, G_{A} is the gain of the bi-directional amplifier and φ is the path additional constant phase shift. So the shifting phase θ which is archived in this phase shifting unit, is

$$\theta = \varphi \pm \tan^{-1}\left(\pm \frac{k_{\mathrm{I}} v_{\mathrm{I}}}{k_{\mathrm{Q}} v_{\mathrm{Q}}}\right). \tag{12}$$

In this phase shifting unit, there exists unreachable phase angle regions because the maximum attenuation response of actual DSA is up to 31.75dB, which cannot reach the zero voltage level. When one path is set as maximum signal (e.g. $\max(k_{\mathrm{I}} v_{\mathrm{I}})$) and another path has the minimum signal (e.g. $\min(k_{\mathrm{Q}} v_{\mathrm{Q}})$), the phase error θ_{error} caused by unreachable phase angle region is 1.52°, calculated by using (12). However, only a few signal vectors are located in this unreachable region, which has no effect on the phase resolution. Because this vector-sum phase shifting unit has lots of available output signal vectors, the calibration of the phase shifting unit is necessary to simplify control program. In calibration process, 256 phase shifting values with lowest amplitude fluctuation, are selected and pre-saved in one table with 8-bit storage depth in controlling FPGA. The measured results of the phase error of phase shifting unit is illustrated in Fig. 7. After the calibration of the PSN, the actual RMS phase shifting error is measured within 0.62° at each set phase. The RMS amplitude fluctuation of phase shifting unit in the whole phase range is 0.13dB, which is shown in Fig. 7.

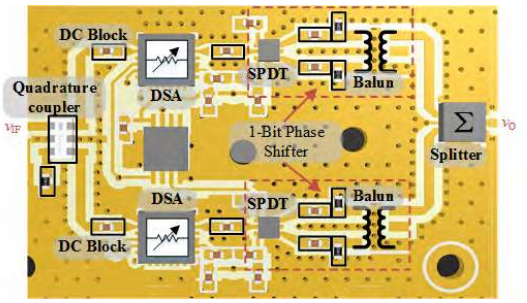

FIGURE 6. The layout of the proposed phase shifting unit.

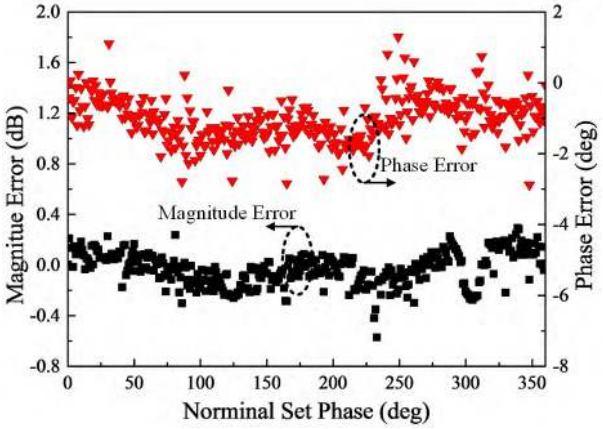

FIGURE 7. The measured phase error and magnitude fluctuation of phase shifting unit at each set phase.

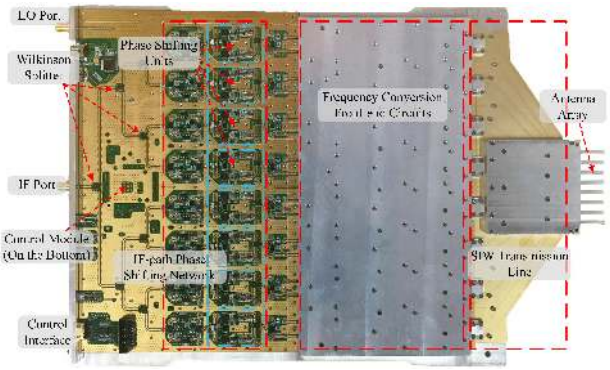

FIGURE 8. The photograph of proposed sub-array without the metal cover of the IF-path phase shifting network.

According to the antenna array theory [28], to prevent the grating lobe of the beam, the distance between adjacent antennas is less than 3/4 wavelength. In this phased array, in order to satisfy the thermal dissipation of the RF front-end when transmitting higher power in each RF chain, the distance between adjacent RF chains is expanded to build the circuits layout more reasonable. Thus, as shown in Fig. 3 and Fig. 8, the phase inconsistence, which affects final beamforming pattern, is introduced between different RF chains. In order to keep consistency of each RF chain, unequal IF phase delay

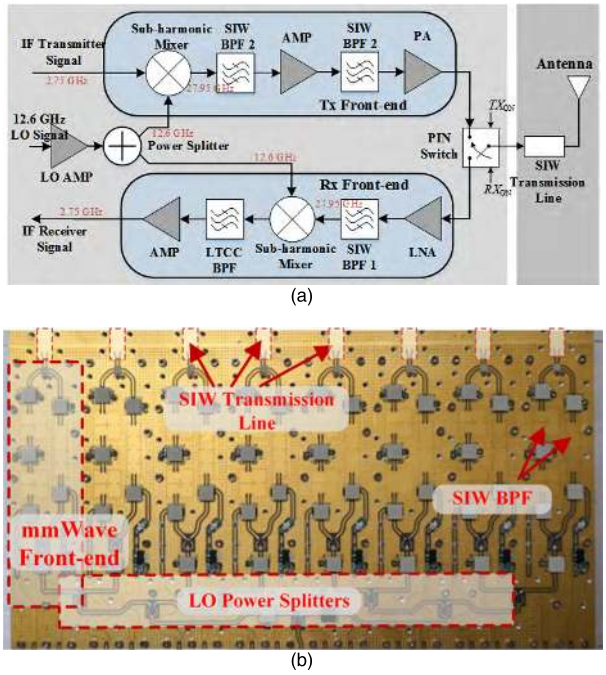

FIGURE 9. (a)The schematic of the one front-end chain circuit. (b) The photograph of front-end circuits in one phased sub-array.

paths are used to increase path length of the intermediate RF chains, that is called path compensation.

Two control modes with different control words length are supported in the phased array. The standard mode can be used for flexible beamforming by setting the phase and amplitude of each chain separately. While the fast mode can be used in beam fast switching application with linear phase precoding. In both modes, the switching between transmitter (Tx) and receiver (Rx) of each chain can be independently adjusted.

2) FREQUENCY CONVERSION FRONT-END DESIGN

In the HBF communication system, the front-end circuits can provide enough signal amplitude gain and linearly-transmitted power in transmitter, as well as the low noise figure in receiver. This front-end circuit contains RF switch, low noise amplifier (LNA), power amplifier (PA), sub-harmonic mixers and SIW bandpass filter (BPF), which is shown in Fig. 9(a). With this sub-harmonic mixer, the frequency required by the RF LO becomes half of the original frequency, which is 12.6GHz in this design. Therefore, it significantly reduces the design difficulty and the cost of the LO subsystem. In transmitter, one driver amplifier is used at mmWave band to drive the PA to output high linear power. In receiver, the gain block is located at IF frequency band after the signal down-conversed for low gain fluctuation. As shown in Fig. 9(b), due to the limited space of the circuits layout, there are two kinds of SIW BPF for filtering out the image side-band and LO leakage. These SIW BPF are four-stage Chebyshev response filter with 2.5GHz bandwidth at 28GHz. The SIW BPFs used in Tx or Rx chain can reach 32dB LO leakage suppression at 25.2GHz and get image

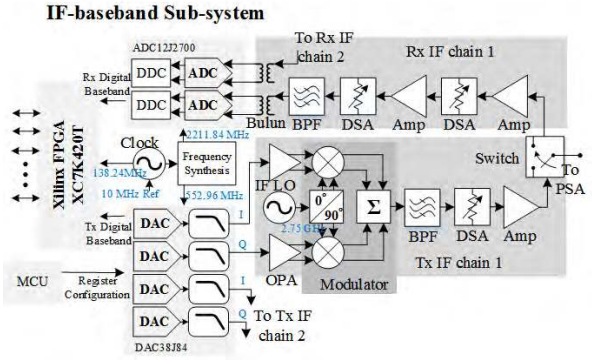

FIGURE 10. The schematic of the IF-baseband subsystem.

side-band rejection of 70dB. Moreover, the substrate integrated waveguide (SIW) transmission lines are used to connect the half wavelength spacing antenna array and the front-end circuits. The SIW transmission line has the advantages of low insertion loss, compact size and easily integration. The radiation antenna element adopted in this transceiver system is a printed planar end-fire dipole antenna with integrated microstrip balun, which is reported in [29]. This end-fire antenna element is promising for millimeter-wave communication due to its high radiation gain, compact size and low cost [30], [31].

B. DESIGN OF IF-BASEBAND SUBSYSTEM

In the IF-baseband subsystem, there are four digitized chains which are distributed in two baseband modules and one 4-chain IF transceiver module. The simplified block diagram of one IF chain with baseband unit in this subsystem is shown in Fig. 10. In transmitter, the differential operational amplifier (OPA) not only converts the single-ended baseband signal into the differential signals, but also achieves the suppression of IF LO leakage through the fine tuning of DC bias voltage in I-path and Q-path. The Tx digital baseband signal is converted to IF band by direct up-conversion, and the high out-of-band spurious are filtered out by the surface acoustic wave filter. To satisfy different communication coverage distance, the DSA and gain amplifier are placed on the IF chain to achieve 31dB dynamic range. In the receiver, the ADC directly under-samples the IF signal, and then uses digital frequency down-conversion and filtering to obtain the I/Q baseband signals. This method has the advantage of reducing the size of receiver and avoiding I/Q imbalance caused by analog demodulation and analog baseband processing. In order to avoid distortion of the sampling signal of the ADC, this digital-IF receiver implements a 63dB dynamic range by using two DSAs and two amplifiers in the receiver chain. As shown in Fig. 11, the measured results of the S-parameter at different attenuation level describes the good gain flatness.

C. DESIGN OF LO SUBSYSTEM

The LO subsystem is an important part of the communication transceiver system in mmWave band. The phase noise of

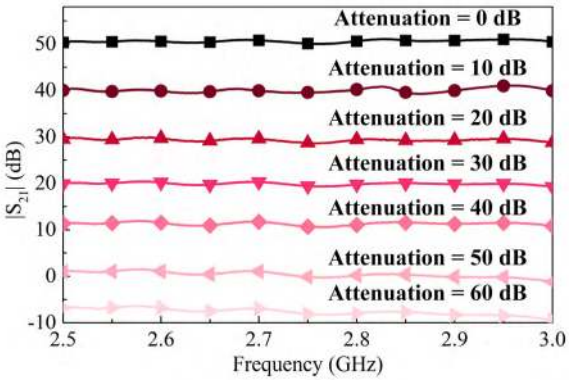

FIGURE 11. The gain fluctuation of IF receiver chain at different attenuation level.

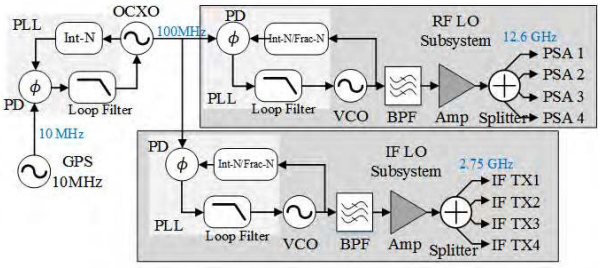

FIGURE 12. The block diagram of proposed LO subsystem in the phased array.

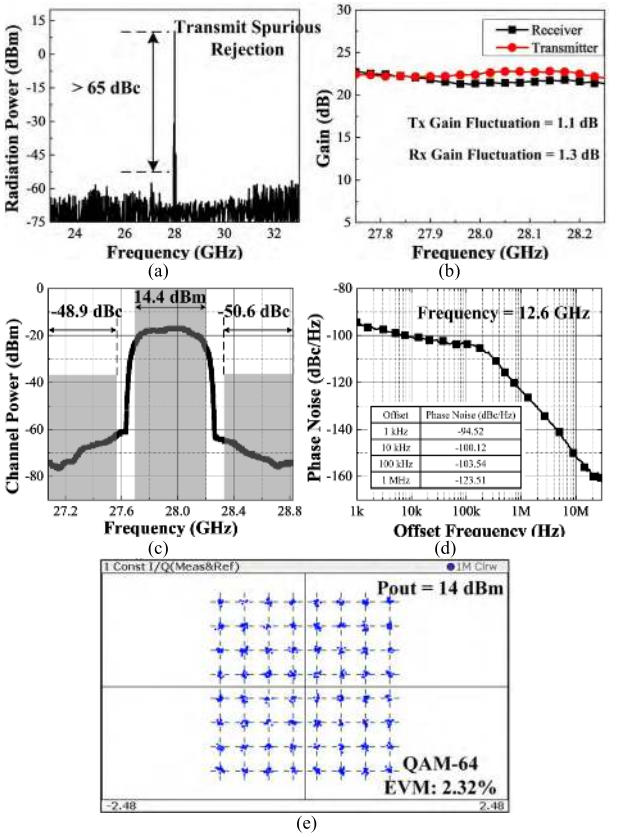

FIGURE 13. The measured RF performance of the phased array. (a) Transmit spurious spectrum. (b) Tx gain response and Rx gain response. (c) Transmit chain power linearity and ACPR. (d) RF LO phase noise at 12.6GHz. (e) EVM and signal constellation.

LO signal has great influence on the digital phase modulation communication system. Because of the frequency conversion, the phase noise of LO signal is mixed into the modulated carrier signal, which deteriorates the signal to noise ratio. In general, as for multi-carrier modulation technology such as orthogonal frequency-division multiplexing (OFDM), the phase noise impacts on its subcarriers orthogonality and inter-carrier interference. Therefore, to inhibit the LO phase noise, a dual-loop PLL structure is used in this system, as shown in Fig. 12. The 10MHz from global positioning system (GPS) source not only is the reference clock of the whole LO subsystem, but also synchronizes different devices. One 100MHz OCXO is utilized as the reference clock of the RF LO and IF LO. Thus, the phase noise of the PLL can be reduced by 10dB, comparing with the one using 10MHz reference clock directly. In addition, one amplifier and one power splitter network are employed to supply enough LO signal power for mixers in multi-chain.

IV. EXPERIMENTAL RESULTS

A. PHASED ARRAY TRANSCEIVER AND BEAM PERFOMANCE TESTS

The HBF communication system signal quality is highly dependent on the transceiver performance. In general, the parameters that demonstrate the RF performance of transceiver include transmitted power linearity, receiver noise, gain fluctuation, spurious suppression and LO phase noise. With the help of signal generator Agilent N8267 and spectrum analyzer Agilent N9030, the measured spectrum of phased array transmitter is shown in Fig. 13(a) and the transmit spurious rejections are more than 65dBc. The measured gain of the transmitter is more than 22dB with the 1.1dB gain fluctuation over 500MHz bandwidth, which is shown in Fig. 13(b). The measured received gain is 21dB and the received gain flatness is 1.3dB over 500MHz channel bandwidth. Moreover, the measured noise figure of the receiver is below 5.3dB.

The transmit power linearity is characterized by adjacent channel power ratio (ACPR). As illustrated in Fig. 13(c), a QAM-64 modulated signal in 28GHz with 500MHz bandwidth is applied at 10-dB back-off from P1dB. The measurement ACPR is −48.9dBc and the practical transmit power of is 14.4dBm. Therefore, for transmitting high peak-average ratio signal such as OFDM signal, each RF transmitter chain can provide 14.4dBm linear power. Through the signal analyzer FSUP, the measured result of the RF LO at 12.6GHz shows great phase noise performance, which is illustrated in Fig. 13(d). The integrated phase noise in the entire offset bandwidth is −48.6dBc, which is superior for high-order modulation signals. To characterize signal quality of whole system, the measured EVM of single-carrier QAM-64 modulation signal is 2.32% and the signal constellation is

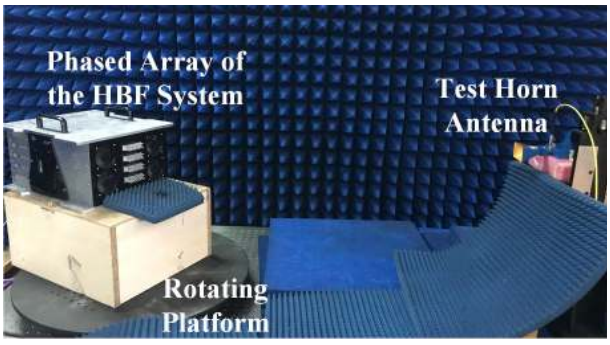

FIGURE 14. Photograph of the designed HBF transceiver array under measurement in the anechoic chamber.

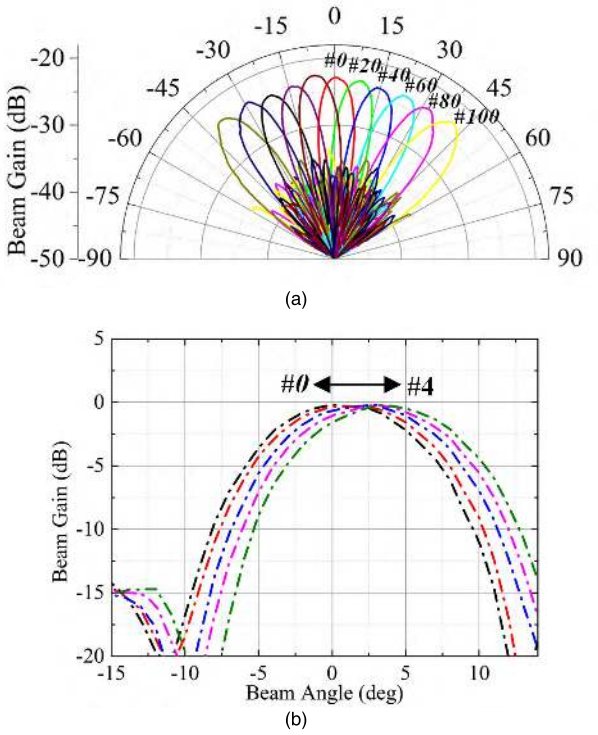

FIGURE 15. Measured horizontal plane beam patterns of the designed HBF array at 28GHz. (b) Measured fine resolution beam steering in the horizontal plane after calibration.

shown in Fig. 13(e). The measured RF performance of this transceiver system are summarized in Table 2.

The beam coverage and beam steering resolution indicate the performance of analog beamforming of the phased array. Fig. 14 shows the designed phased array under beam pattern measurement and beam switching test in the anechoic chamber. In fast control mode, 11 orthogonal beam patterns are selected from all beams to cover the whole space angle range, which is shown in Fig. 15(a). The measured results show that the beam coverage of main beam can reach 90° range in the horizontal plane. In addition, the beam patterns with minimum resolution angle are demonstrated in Fig. 15(b), where the fine beam resolution can be found as 0.6°. With the amplitude weighted in different RF chains, the low

TABLE 2. Measured specifications of transceiver system.

	RX	TX
Frequency (GHz)	28	
IF Bandwidth (MHz)	500	
LO Int. Phase Noise	-48.6 dBc	
Gain (dB)	21	22
Fluctuation (dB)	1.3	1.1
Tx OP1dB (dBm)	-	24.4
Rx NF (dB)	5.3	-
Gain Control Range (dB)	63	31
Phase Control Resolution	1.4° (8-bit)	1.4° (8-bit)

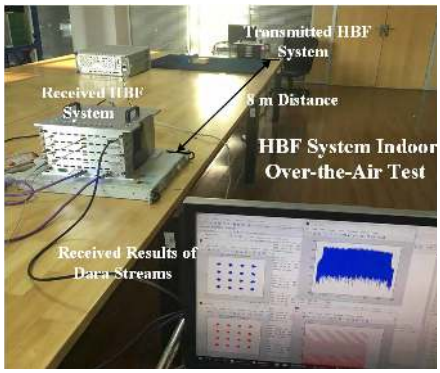

FIGURE 16. Photograph of the HBF system indoor over-the-air MIMO signal transmission test scenario.

side lobe beam pattern can be achieved to further decrease the interference to other UEs. The beam performance of this work and the comparison with other phased array transceivers are summarized in Table 3.

B. OVER-THE-AIRMIMO COMMUNICATION PERFORMANCE TESTS

To verify the performance of this HBF communication system, two identical HBF transceiver systems are employed for the indoor over-the-air signal transmission test. One HBF transceiver system acts as the base station and another acts as the UE. According to the standards of 5G, wideband multi-carriers signal is applied in actual communication system. Therefore, the indoor over-the-air test use 500MHz bandwidth OFDM data streams, whose adopted modulation mode is QAM-16. The indoor test scenario is shown in the Fig. 16. Two HBF transceiver systems are located at the ends of the wooden table, with the distance of 8m. Simultaneously, the PC host shows the real-time demodulated signal constellation, spectrum and correlation peaks of the received signals. Due to the laboratory conditions, the 2×2 MIMO communication test is employed in this system. At first, different signal streams are transmitted by any two of the four digital chains in each test. The signals are radiated into the space through different analog precoding matrix in phased array, respectively. At the receiver, any two of the four digital

TABLE 3. Comparison with other phased array transceiver system.

Reference	Frequency (GHz)	Elements in Array	Tx/Rx[a]	PSN Architecture	Phase Range	Phase Resolution	RMS Phase Error	RMS Mag. Fluctuation	Beam Resolution	EVM
[21]	28	32	Tx and Rx	RF-path phase shifter	360°	5.6°(6-bit)	<4°	<0.7dB	<1°	1.64% QAM-64 (100MHz)
[23]	28	8	Rx	RF-path phase shifter	360°	11.25°(5-bit)	0.4°	0.8dB	4°	-
[32]	28	8	Tx and Rx	RF-path phase shifter	360°	45°(3-bit)	7°	-	14°	2.2% QAM-64 (10MHz)
[33]	28	32	Tx and Rx	RF-path phase shifter	360°	~5°(6-bit)	<1°	<1.5dB	1.4°	-
[34]	28	64	Tx and Rx	RF-path phase shifter	360°	11.25°(5-bit)	5°	0.5dB	3.6°	-
This Work	28	32	Tx and Rx	IF-path vector modulator	360°	1.4° (8-bit)	0.62°	0.13dB	0.6°	1.05% QAM-64 (100 MHz)

[a]Tx means the transmitter array, and Rx means the receiver array.

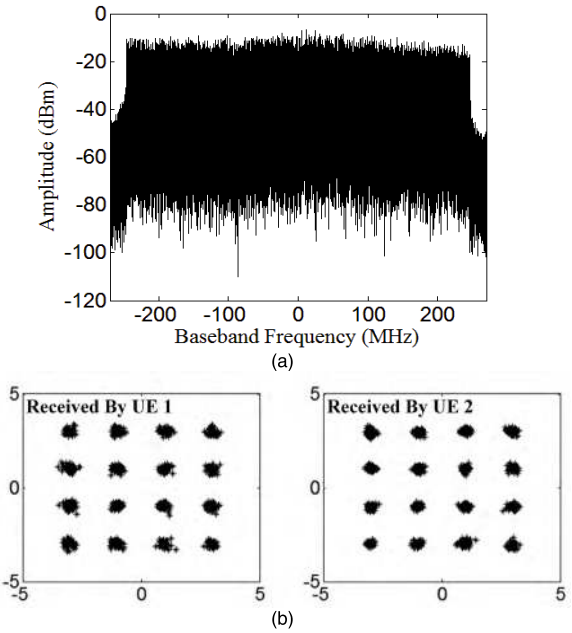

FIGURE 17. (a) The spectrum of received 500MHz OFDM signal. (b) The measured results of received signal constellations of two UEs.

receiver chains, which are equivalent to two UEs, receive the MIMO signals simultaneously. After that, the received signals are down-converted and sampled to baseband units, the sampled spectrum of which is shown in Fig. 17(a). The received signal constellations of the two data streams are demonstrated in Fig. 17(b). The received demodulated signal EVMs of two UEs are 2.58% and 2.34%, respectively. In the ideal case of QAM-16 modulation signal, each data stream can achieve a maximal date rate of 1.9692Gbps. The over-the-air tests verify the feasibility of building a high performance HBF transceiver system for high data rate millimeter-wave cellular communication.

V. CONCLUSION

In this paper, a 32-antenna HBF transceiver system based on high precision phased array for mmWave MIMO communication is developed. This mmWave MIMO HBF transceiver system is operated at 28GHz band with 500MHz signal bandwidth. The HBF system contains four 8-antenna sub-arrays with their IF-baseband subsystems. This paper also analyzes the influence of the RF chain vector error to the final beam pattern and designs a high precision phased array based on the analysis. Measurement results show that the beam coverage range in 28GHz is more than 90° with a 0.6° beam resolution. With carefully design of mmWave RF front-end circuits, the proposed transceiver system achieves great RF performance. Through the two streams indoor over-the-air MIMO communication test, the high data rate mmWave communication of this HBF is verified, and as a result, the received EVMs of two UEs are 2.58% and 2.34%, respectively.

REFERENCES

[1] T. S. Rappaport, S. Sun, R. Mayzus, H. Zhao, Y. Azar, K. Wang, G. N. Wong, J. K. Schulz, M. Samimi, and F. Gutierrez, "Millimeter wave mobile communications for 5G cellular: It will work!" *IEEE Access*, vol. 1, pp. 335–349, 2013.

[2] W. Roh, J.-Y. Seol, J. Park, B. Lee, J. Lee, Y. Kim, J. Cho, K. Cheun, and F. Aryanfar, "Millimeter-wave beamforming as an enabling technology for 5G cellular communications: Theoretical feasibility and prototype results," *IEEE Commun. Mag.*, vol. 52, no. 2, pp. 106–113, Feb. 2014.

[3] S. Han, I. Chih-lin, Z. Xu, and C. Rowell, "Large-scale antenna systems with hybrid analog and digital beamforming for millimeter wave 5G," *IEEE Commun. Mag.*, vol. 53, no. 1, pp. 186–194, Jan. 2015.

[4] B. Yang, Z. Yu, J. Lan, R. Zhang, J. Zhou, and W. Hong, "Digital beamforming-based massive MIMO transceiver for 5G millimeter-wave communications," *IEEE Trans. Microw. Theory Techn.*, vol. 66, no. 7, pp. 3403–3418, Jul. 2018.

[5] S. He, C. Qi, Y. Wu, and Y. Huang, "Energy-efficient transceiver design for hybrid sub-array architecture MIMO systems," *IEEE Access*, vol. 4, pp. 9895–9905, 2017.

[6] Y. Lin, S. Jin, M. Matthaiou, and X. You, "Transceiver design with UCD-based hybrid beamforming for millimeter wave massive MIMO," *IEEE Trans. Commun.*, vol. 67, no. 6, pp. 4047–4061, Jun. 2019.

[7] X. Liu, Q. Zhang, W. Chen, H. Feng, L. Chen, F. M. Ghannouchi, and Z. Feng, "Beam-oriented digital predistortion for 5G massive MIMO hybrid beamforming transmitters," *IEEE Trans. Microw. Theory Techn.*, vol. 66, no. 7, pp. 3419–3432, Jul. 2018.
[8] Y. Ren, Y. Wang, C. Qi, and Y. Liu, "Multiple-beam selection with limited feedback for hybrid beamforming in massive MIMO systems," *IEEE Access*, vol. 5, pp. 13327–13335, 2017.
[9] T. E. Bogale, L. B. Le, A. Haghighat, and L. Vandendorpe, "On the number of RF chains and phase shifters, and scheduling design with hybrid analog-digital beamforming," *IEEE Trans. Wireless Commun.*, vol. 15, no. 5, pp. 3311–3326, May 2016.
[10] F. Sohrabi and W. Yu, "Hybrid digital and analog beamforming design for large-scale antenna arrays," *IEEE J. Sel. Topics Signal Process.*, vol. 10, no. 3, pp. 501–513, Apr. 2016.
[11] J. Du, W. Xu, H. Shen, X. Dong, and C. Zhao, "Hybrid precoding architecture for massive multiuser MIMO with dissipation: Sub-connected or fully connected structures?" *IEEE Trans. Wireless Commun.*, vol. 17, no. 8, pp. 5465–5479, Aug. 2018.
[12] S.-F. Chuang, W.-R. Wu, and Y.-T. Liu, "High-resolution AoA estimation for hybrid antenna arrays," *IEEE Trans. Antennas Propag.*, vol. 63, no. 7, pp. 2955–2968, Jul. 2015.
[13] J. Zhang, Y. Huang, J. Wang, and L. Yang, "Hybrid precoding for wideband millimeter-Wave systems with finite resolution phase shifters," *IEEE Trans. Veh. Technol.*, vol. 67, no. 11, pp. 11285–11290, Nov. 2018.
[14] J.-C. Chen, "Hybrid beamforming with discrete phase shifters for millimeter-wave massive MIMO systems," *IEEE Trans. Veh. Technol.*, vol. 66, no. 8, pp. 7604–7608, Aug. 2017.
[15] M. Li, Z. Wang, H. Li, Q. Liu, and L. Zhou, "A hardware-efficient hybrid beamforming solution for mmWave MIMO systems," *IEEE Wireless Commun.*, vol. 26, no. 1, pp. 137–143, Feb. 2019.
[16] Z. Wang, M. Li, Q. Liu, and A. L. Swindlehurst, "Hybrid precoder and combiner design with low-resolution phase shifters in mmWave MIMO systems," *IEEE J. Sel. Topics Signal Process.*, vol. 12, no. 2, pp. 256–269, May 2018.
[17] G. Li, J. Wu, Z. Chen, X. Luo, T. Tang, and Z. Xu, "Performance analysis and evaluation for active antenna arrays under three-dimensional wireless channel model," *IEEE Access*, vol. 6, pp. 19131–19139, 2018.
[18] X. Cheng, Y. Yao, T. Tomura, J. Hirokawa, T. Yu, J. Yu, and X. Chen, "Millimeter-wave frequency beam scanning array with a phase shifter based on substrate-integrated-waveguide," *IEEE Access*, vol. 6, pp. 47408–47414, 2018.
[19] P. F. Kou and Y. J. Cheng, "Ka-band low-sidelobe-level slot array leaky-wave antenna based on substrate integrated nonradiative dielectric waveguide," *IEEE Antennas Wireless Propag. Lett.*, vol. 16, pp. 3075–3078, 2017.
[20] J. Brady, J. Hogan, and A. Sayeed, "Multi-beam MIMO prototype for real-time multiuser communication at 28 GHz," in *Proc. IEEE Globecom Workshops (GC Wkshps)*, Washington, DC, USA, Dec. 2016, pp. 1–6.
[21] K. Kibaroglu, M. Sayginer, and G. M. Rebeiz, "A low-cost scalable 32-element 28-GHz phased array transceiver for 5G communication links based on a 2×2 beamformer flip-chip unit cell," *IEEE J. Solid-State Circuits*, vol. 53, no. 5, pp. 1260–1274, May 2018.
[22] M. Nikfalazar, C. Kohler, A. Wiens, A. Mehmood, M. Sohrabi, H. Maune, J. R. Binder, and R. Jakoby, "Beam steering phased array antenna with fully printed phase shifters based on low-temperature sintered BST-composite thick films," *IEEE Microw. Wireless Compon. Lett.*, vol. 26, no. 1, pp. 70–72, Jan. 2016.
[23] R. Garg and A. S. Natarajan, "A 28-GHz low-power phased-array receiver front-end with 360° RTPS phase shift range," *IEEE Trans. Microw. Theory Techn.*, vol. 65, no. 11, pp. 4703–4714, Nov. 2017.
[24] M. Sayginer and G. M. Rebeiz, "An eight-element 2–16-GHz programmable phased array receiver with one, two, or four simultaneous beams in SiGe BiCMOS," *IEEE Trans. Microw. Theory Techn.*, vol. 64, no. 12, pp. 4585–4597, Dec. 2016.
[25] A. Li and C. Masouros, "Energy-efficient SWIPT: From fully digital to hybrid analog-digital beamforming," *IEEE Trans. Veh. Technol.*, vol. 67, no. 4, pp. 3390–3405, Apr. 2018.
[26] C. Liu, Q. Li, Y. Li, X.-D. Deng, H. Tang, R. Wang, H. Liu, and Y.-Z. Xiong, "A Ka-band single-chip SiGe BiCMOS phased-array transmit/receive front-end," *IEEE Trans. Microw. Theory Techn.*, vol. 64, no. 11, pp. 3667–3677, Nov. 2016.
[27] F. Hutu, D. Cordeau, and J.-M. Paillot, "2.4 GHz antenna array using vector modulator-based active phase shifters for beamforming," *IET Microw., Antennas Propag.*, vol. 5, no. 2, pp. 245–254, Jan. 2011.
[28] W. Hong, Z. H. Jiang, C. Yu, J. Zhou, P. Chen, Z. Yu, H. Zhang, B. Yang, X. Pang, M. Jiang, Y. Cheng, M. K. T. Al-Nuaimi, Y. Zhang, J. Chen, and S. He, "Multibeam antenna technologies for 5G wireless communications," *IEEE Trans. Antennas Propag.*, vol. 65, no. 12, pp. 6231–6249, Dec. 2017.
[29] B. Yang, Z. Yu, Y. Dong, J. Zhou, and W. Hong, "Compact tapered slot antenna array for 5G millimeter-wave massive MIMO systems," *IEEE Trans. Antennas Propag.*, vol. 65, no. 12, pp. 6721–6727, Dec. 2017.
[30] M. Sun, X. Qing, and Z. N. Chen, "60-GHz end-fire fan-like antennas with wide beamwidth,"178 *IEEE Trans. Antennas Propag.*, vol. 61, no. 4, pp. 1616–1622, Apr. 2013.
[31] B. K. Tehrani, B. S. Cook, and M. M. Tentzeris, "Inkjet printing of multilayer millimeter-wave Yagi-Uda antennas on flexible substrates," *IEEE Antennas Wireless Propag. Lett.*, vol. 15, pp. 143–146, 2015.
[32] H.-T. Kim, B.-S. Park, S.-M. Oh, S.-S. Song, J.-M. Kim, S.-H. Kim, T.-S. Moon, S.-Y. Kim, J.-Y. Chang, S.-W. Kim, W.-S. Kang, S.-Y. Jung, G.-Y. Tak, J.-K. Du, Y.-S. Suh, and Y.-C. Ho, "A 28 GHz CMOS direct conversion transceiver with packaged antenna arrays for 5G cellular system," in *Proc. IEEE Radio Freq. Integr. Circuits Symp. (RFIC)*, Honolulu, HI, USA, Jun. 2017, pp. 69–72.
[33] B. Sadhu, Y. Tousi, J. Hallin, S. Sahl, S. Reynolds, Ö. Renström, K. Sjögren, O. Haapalahti, N. Mazor, B. Bokinge, G. Weibull, H. Bengtsson, A. Carlinger, E. Westesson, J.-E. Thillberg, L. Rexberg, M. Yeck, X. Gu, D. Friedman, and A. Valdes-Garcia, "7.2 A 28 GHz 32-element phased-array transceiver IC with concurrent dual polarized beams and 1.4 degree beam-steering resolution for 5G communication," in *Proc. IEEE Int. Solid-State Circuits Conf. (ISSCC)*, San Francisco, CA, USA, Feb. 2017, pp. 128–129.
[34] G. Raney, B. Unruh, R. Lovestead, and B. Winther, "64-Element 28 gigahertz phased array 5G prototyping platform," in *Proc. 11th Global Symp. Millim. Waves (GSMM)*, Boulder, CO, USA, May 2018, pp. 1–4.

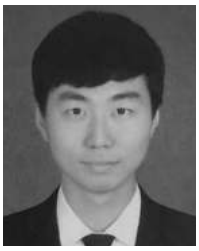

RUOQIAO ZHANG received the B.S. degree in electrical engineering from Southeast University, Nanjing, China, in 2014, where he is currently pursuing the Ph.D. degree in electromagnetic field and microwave technology. His current research interests include tunable circuit components, active antenna array systems, microwave and millimeter-wave transceiver systems, beamforming networks, and phased arrays for mobile communication.

JIANYI ZHOU (M'05) received the B.S., M.S., and Ph.D. degrees from Southeast University, Nanjing, China, in 1993, 1996, and 2001, respectively. In 1996, he joined the Faculty of the Department of Radio Engineering, Southeast University, as an Assistant Professor, where he became a Lecturer, in 1998, an Associate Professor, in 2001, and a Professor, in 2005. His current research interest includes RF circuits and systems in mobile communications.

JI LAN received the B.S. and M.S. degrees in electrical engineering from Southeast University, Nanjing, China, in 2013 and 2015, respectively, where he is currently pursuing the Ph.D. degree in electromagnetic field and microwave technology. His current research interests include microwave circuits, transceiver systems, and antennas in mobile communication.

BINQI YANG received the B.S., M.S., and Ph.D. degrees in information engineering from Southeast University, Nanjing, China, in 2013, 2015, and 2019, respectively, where he is currently pursuing the Ph.D. degree in electromagnetic field and microwave technology. In 2013, he joined the State Key Laboratory of Millimeter Waves, Southeast University. His current research interests include planar filters, millimeter-wave antennas, microwave and millimeter-wave circuits and transceiver systems, beam-forming networks, and phased arrays for mobile communications.

ZHIQIANG YU (M'13) received the B.S. degree from the Nanjing University of Science and Technology, Nanjing, China, in 2002, and the Ph.D. degree from Southeast University, Nanjing, in 2013. From 2002 to 2007, he was a Member of Research Staff involved with airborne radar transmitters with the Nanjing Institute of Electronics, CETC, Nanjing. He is currently a Lecturer with the School of Information Science and Engineering, Southeast University. His current research interest includes microwave and millimeter-wave circuits and system design.